https://doi.org/10.5194/egusphere-2026-4590
Preprint. Discussion started: 21 August 2026

Impact of urban-industrial air pollution on chemically reactive greenhouse gases is highly sensitive to organic nitrate formation

Calum P. Wilson[1] and Michael J. Prather[1]

[1]Department of Earth System Science, University of California, Irvine, Irvine, 92697, United States of America

Correspondence to: Calum P. Wilson (calumw@uci.edu)

Abstract. We compute net tropospheric ozone production (P-O_3) and methane oxidation (L-CH_4) caused by 45 days of South Korean emissions using a chemistry-transport model (CTM) and a hybrid modelling system (HMS). The CTM has global 1° x 1° resolution; the HMS has detailed chemical mechanisms and a refined regional grid (0.1° x 0.1°), but simplified, staged transport. The emissions cause +22.1 Gmol P-O_3 and +2.0 Gmol L-CH_4 in the CTM *vs*. +31.2 Gmol P-O_3 and +4.3 Gmol L-CH_4 in the HMS. Differences are attributed to lower volatile organic compound (VOC) reactivity in the CTM, thus decreased organic nitrate export to the free troposphere. Time-integrated O_3 mass perturbations (δO_3) are similar in both models and constitute a globally-averaged +0.03 DU summertime O_3 enhancement. Due to contrasting L-CH_4, the net steady-state effective radiative forcing sustained by the emissions is +0.49 mW m^{-2} in the CTM and -0.25 mW m^{-2} in the HMS.

1 Introduction

Tropospheric ozone (O_3) and methane (CH_4) are short-lived greenhouse gases whose atmospheric abundances have risen since the preindustrial era (Szopa *et al*., 2023). Methane growth has been driven primarily by fossil fuel and agricultural emissions (Saunois *et al*., 2025), likely offset by growth in the main CH_4 sink, the hydroxyl radical (OH) (Isaksen and Hov, 1986; Stevenson *et al*., 2020). Ozone is both produced and destroyed through atmospheric chemistry. Ozone growth since the 1980s is attributed to intensified precursor emissions including nitrogen oxides (NO_x), carbon monoxide (CO), and volatile organic compounds (VOCs), which are driven by industrialisation, most recently across Asia (Gaudel *et al*., 2018; Ziemke *et al*., 2019). In this work, we investigate the global CH_4 and O_3 perturbations caused by anthropogenic air pollution from South Korea using a global chemistry-transport model (CTM), and compare the results with those from a regional, hybrid modelling system (HMS; Wilson and Prather, 2026) with refined horizontal resolution and highly detailed chemical mechanisms.

Greenhouse gas budgets for O_3 and CH_4 are sensitive to the distribution of polluted air in the free troposphere (Guo *et al*., 2023). Chemistry-transport models are effective tools for computing CH_4 and O_3 budgets in response to pollution because they seamlessly integrate the transport and chemistry of the emissions. However, the computational cost of global-scale modelling requires model compromises such as simplified chemical mechanisms and coarsened spatial resolution. Our work with the HMS addressed these issues via a regional study limited to South Korea with refined boundary-layer horizontal resolution and a nearly complete set of chemical reactions. Pollution plumes transported beyond the model domain were treated in a

https://doi.org/10.5194/egusphere-2026-4590
Preprint. Discussion started: 21 August 2026

subsequent box modelling stage, after which residual pollutants were linearly dispersed. This approach captured the budget terms over the full lifespan of the emissions, but introduced discontinuities between the modelling stages and did not simulate plume trajectories beyond South Korea.

We use a standard UC Irvine CTM simulation (Prather, 2024; Prather and Zhu, 2024; Prather, 2025) with an added 45-day South Korean emission perturbation at the 10% level of anthropogenic emissions used in the HMS work. We accumulate the total loss of CH_4 (L-CH_4, Gmol) from those added emissions as well as the integrated O_3 perturbation (Gmol days). Deriving total net production of O_3 (P-O_3, Gmol) from the O_3 perturbation (Gmol days) requires knowledge of the O_3 lifetime (days), which varies from 6 to 26 days based on altitude and season (Prather and Zhu, 2024). We calculate these lifetimes for the Pacific troposphere by simulating the decay of artificial O_3 releases from four vertically stacked boxes downwind of South Korea in May.

We discuss the modelling parameters and O_3 lifetime determination in Section 2, derive the budgets and radiative forcings in Section 3, and present our findings in Section 4.

2 Methodology

2.1 Chemistry-transport modelling

The control CTM run uses the same meteorology, chemical mechanisms, and emission inventories as described in Prather (2025). The run consists of a 92-day study period 01 May to 01 August (midnight UTC) using the available meteorology for year 2000 and fully spun up initial conditions for 01 May 2000. The control inventories include the MEGAN-MACC biogenic emissions (Sindelarova *et al*., 2014; Guenther *et al*., 2012) and CMIP6 emissions for anthropogenic, biofuel, and biomass burning (Hoesly *et al.*, 2018) for the following species: carbon monoxide (CO), nitric oxide (NO), ethane (C_2H_6), 'alkane' (propane and higher alkanes), 'alkene' (ethene and higher alkenes), formaldehyde (HCHO), acetaldehyde (CH_3CHO), acetone (CH_3COCH_3), and isoprene (C_5H_8). Lightning NO emissions are also included. The CTM tropospheric chemical mechanism includes 24 species and 86 reactions in addition to dry deposition and washout.

The emission run includes the KORUS v5 anthropogenic (Woo *et al.*, 2020) and GFED5 biomass burning (Chen *et al.*, 2023) inventories used in the HMS. These emissions are converted from SAPRC format (Carter, 2010) to CTM species (see Table 1). Lumped SAPRC species are each assigned a single molecular weight based on the most abundant component (see Wilson and Prather, 2026) and converted from mol s^{-1} to kg m^{-2} s^{-1} units. Aromatic species (ARO1 and ARO2) are not included in the CTM chemistry, but here we add these into the 'Alkene' emission category as they generally oxidise to form alkenyl products. The 45-day "KORUS-AQ" emission period follows the timeframe of the Korea-US Air Quality mission from 01 May to 14 June (midnight UTC) and is followed by a spin-down period for the remaining 47 days simulated in the control run. After day 92, we have reached about 97% of the total chemical impact of the emission period and can easily extrapolate the residual chemical perturbations driven by long-lived CO chemistry.

https://doi.org/10.5194/egusphere-2026-4590
Preprint. Discussion started: 21 August 2026

Table 1: The mapping of KORUS v5 and GFED5 emission inventories (01 May - 15 June) to UCI CTM species.

UCI CTM surrogate species	SAPRC emitted species (MCM surrogates)	CTM cumulative emissions (kt)
NO	NO	92
NO_2	NO_2	19
CO	CO	205
Isoprene	Isoprene	0.5
MVKMACR	Methyl vinyl ketone Methacrolein Total	0.0 0.0 0.5
Formaldehyde	Formaldehyde	1.1
Acetaldehyde	Acetaldehyde Glyoxal Methylglyoxal Benzaldehyde Diacetyl RCHO (Propanaldehyde) Total	0.6 0.2 0.1 0.0 0.0 0.3 1.2
Ethane	ALK1 (Ethane)	3.7
Alkane	ALK2 (Propane) ALK3 (Butanes) ALK4 (3/4 Pentanes + 1/4 Hexanes) ALK5 (Heptanes) Acetone Methyl ethyl ketone Total	4.8 3.3 10.5 15.1 0.4 0.6 34.7
Alkene	Ethene OLE1 (Propene) OLE2 (1,3-Butadiene) ARO1 (1/3 Benzene + 2/3 Toluene) ARO2 (2/3 Xylenes + 1/3 Trimethylbenzenes) Total	8.3 4.1 5.5 34.4 18.3 70.6

KORUS v5 emissions (Woo et al., 2020) were converted from mol s^{-1} emissions to kg m^{-2} s^{-1} emissions. Moles are converted to mass using the molecular weights of the emitted species, and emissions are re-gridded to 0.5°x0.5° in CMIP6 format for the CTM. Lumped SAPRC species are represented in the HMS by MCM surrogates (parenthesised), whose molecular masses are used in the CTM unit conversion. Emissions from oceanic grid cells in the 0.1°x0.1° HMS model are not included in the Wilson and Prather (2026) calculations, nor the CTM calculations here.

https://doi.org/10.5194/egusphere-2026-4590
Preprint. Discussion started: 21 August 2026

2.2 Hybrid modelling system

The goal of the HMS is to simulate the full life cycle of the KORUS-AQ air pollution emissions, with best available chemical mechanisms from MCM v3.3.1 (Bloss et al., 2005; Jenkin et al., 1997; Jenkin et al., 2003; Jenkin et al., 2015; Saunders et al., 2003) while tracking the resulting CH_4 and O_3 budget perturbations. The HMS consists of three separate stages that emulate the chemical evolution of pollution instead of the continuous chemistry and 3D transport afforded by the CTM. As described in Wilson and Prather (2026), "the boundary layer-residual layer (BL-RL) stage processes the emissions, photochemistry, deposition, aerosol reactivity, and transport over terrestrial South Korea at 0.1°×0.1° with hourly resolution. The plume (PL) stage continues to integrate the chemistry of air masses from the BL-RL stage as they are transported offshore, simulating offshore pollution plumes observed by aircraft. After three days of chemical aging in non-diluting plumes, the pollution remnants are dispersed (DP stage) into the background atmosphere and integrated until the pollution disappears." Ozone lifetimes in the HMS are computed for a four-layer (2, 4, 6, and 8 km), statically maintained background atmosphere composition constrained by observations from the Atmospheric Tomography mission (ATom).

2.3 Structural model differences

Structural differences between the two models inevitably bias the budgets with respect to one another. For example, the CTM mixes emissions into 10,000 km^2 grid cells *vs*. 100 km^2 in HMS, thereby missing the extreme non-linear chemistry near source regions. Emitting NO_x pollution over larger areas reduces NO_x saturation and O_3 titration (Zakoura and Pandis, 2018; Li *et al.*, 2023) and increases the NO_x-efficiency of P-O_3 and L-CH_4 (Charlton-Perez *et al.*, 2009; Wild *et al.*, 2004). The CTM continuously dilutes pollution plumes through resolved divergent flow and other unresolved mixing. In contrast, pollution plumes in the HMS remain isolated in the free troposphere for 0-3 days before they are instantly mixed into the background. The varying atmospheric conditions that drive chemistry downwind of the boundary layer (*i.e.* temperature, pressure, water vapor, J-values) are not resolved in the HMS.

The chemistry in the UCI CTM lacks aromatic mechanisms and does not accurately represent higher-mass VOCs and their diverse oxidised intermediates. The only fast-reacting VOC in the CTM is the alkene species (C_2H_4), used as a surrogate for all alkene and aromatic emissions. Thus, the CTM underrepresents VOC-OH reactivity and O_3 production, thereby sustaining NO_x-saturated conditions at lower NO_x abundance. Another consequence of reduced VOC reactivity is much lower production of organic nitrates (Fischer *et al*., 2014), represented in the CTM only by peroxyacetyl nitrate (PAN). The HMS includes 94 additional peroxyacyl nitrate species, 340 alkyl nitrates, and 57 aromatic nitrates. Organic nitrates sequester NO_x and deliver it to the remote troposphere where it is more effective at increasing P-O_3 and L-CH_4 (Singh, 1987; Hudman *et al*., 2004; Fischer *et al.*, 2010).

We compare probability distributions of vertical profiles (lower, median, and upper quartiles) from the control CTM run with *in situ* observations from the 10 s merge DC-8 KORUS-AQ data (KORUS-AQ Science Team, 2019) alongside the HMS boundary layer data (Fig. 1). At each CTM level, quantiles are extracted from 45 daily average values over the 6 CTM grid

https://doi.org/10.5194/egusphere-2026-4590
Preprint. Discussion started: 21 August 2026

cells that lie predominantly over South Korea (126.5°E-129.8°E and 34.8°N-38.1°N). The HMS boundary-layer data comprises 45x24 instantaneous hourly data points for 1092 terrestrial grid-cells. The quantiles extracted from this data are mass-weighted to account for fluctuations in boundary-layer height. Aircraft quantiles are computed from all South Korean data (55,696 flight segments) within separate vertical bins matching the CTM edge-level pressures. The models and observations show good agreement on NO_x and O_3. Ozone disagreement near the surface is explained by daytime-only sampling by the aircraft, positively biasing the observations below 2 km (see Fig. 6 from Crawford *et al.*, 2021). Both models underestimate CO, HCHO, CH_3CHO, and PAN, as did other modelling studies (*e.g.*, supplement from Oak *et al.*, 2019; Table 4 from Kim *et al.*, 2024). Model underestimates are more pronounced in the CTM, where HCHO, CH_3CHO, and PAN in the lowest 2 km are lower than observations by a factor of 2. This is indicative of underestimated VOC reactivity, which reduces PAN abundance due to feedbacks on O_3 and NO_2 (Fischer et al., 2014). Differences between HMS and CTM also reflect the HMS choice of clean-air background that excludes the influence of transboundary air pollution on South Korea (Miyazaki *et al.*, 2019; Kim *et al.*, 2024).

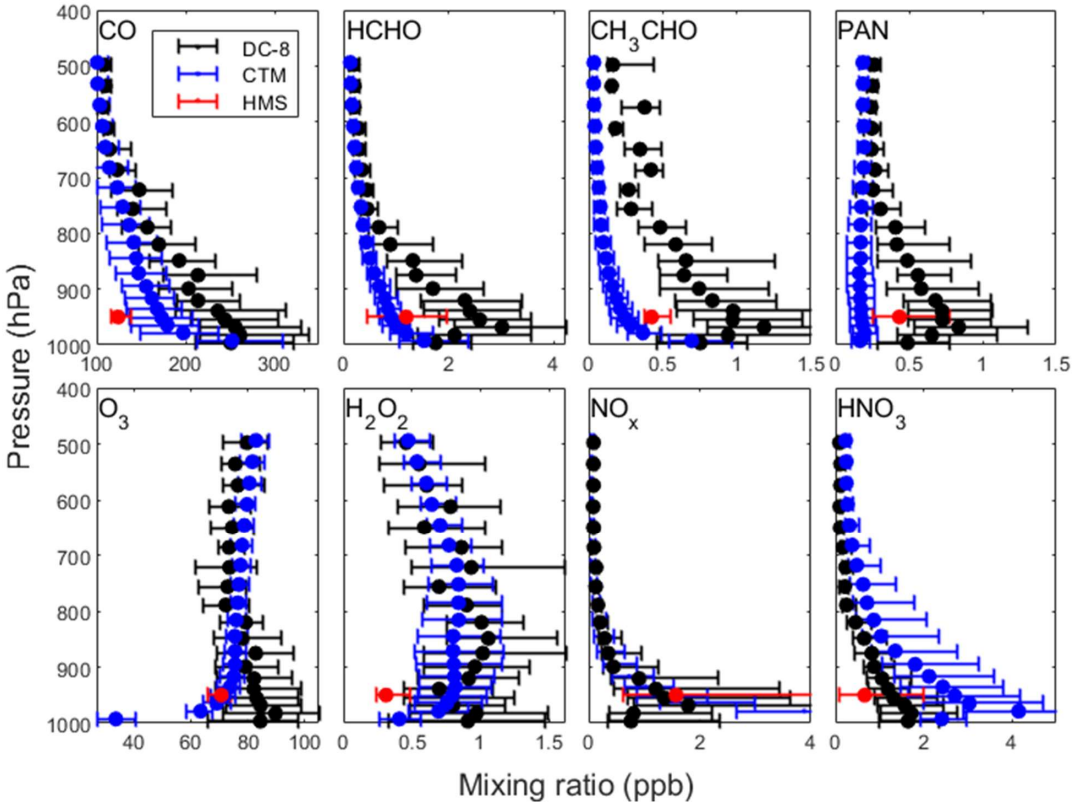

Figure 1: Vertical profiles of observed (black) and CTM (blue) mole fractions with HMS boundary-layer data. Dots are medians and horizontal bars are lower and upper quartiles KORUS-AQ in situ DC-8 data were sampled from 08:00 to 18:00 UTC+09 between the mean

https://doi.org/10.5194/egusphere-2026-4590
Preprint. Discussion started: 21 August 2026

edge-level pressures of the CTM on 21 flight days over South Korea (see Figure 3 from Crawford et al., 2021). Model data (CTM: daily diurnal averages; HMS: hourly) are sampled every day from 01 May to 15 June starting 00:00 UTC (HMS: 15:00 UTC) in a box from 126.5°E-129.8°E and 34.8°N-38.1°N.

2.4 Ozone lifetime in the CTM

We estimate the perturbation lifetime of tropospheric O_3 in a broad box (29.2-49.3°N, 128.8-149.1°E) enveloping the region of largest O_3 perturbations in the CTM. The box is vertically partitioned into four pressure intervals by level number: 1000-800 hPa (L1-10), 800-600 hPa (L11-16), 600-400 hPa (L17-21), and 400-300 hPa (L22-24). Beginning 01 May 2000 at 00:00 UTC, we release a 'puff' of O_3 into each vertical box partition, adding +10% O_3 mass to each constituent 3D cell. We integrate 61 days of chemistry-transport against a control run. The O_3 lifetime in each vertical partition is computed from the time-integral of the O_3 mass perturbation divided by the initial perturbation mass. The tail of the O_3 decay beyond 61 days is extrapolated by a least-squares exponential fit using the last 10 days of data. The O_3 lifetimes in the four partitions (lowest to highest altitude) are 11.4, 13.7, 15.9, and 19.1 days. After 20 days, the CTM O_3 perturbations at all levels decay with an e-fold of around 13 days (see Fig. 2) as expected from vertical mixing rates in the troposphere (Prather 2025). These CTM lifetimes contain the feedbacks from chemistry and transport, whereas the lifetimes in the HMS, 5.8, 10.8, 17.9, and 24.2 days, were computed at fixed altitudes of 2 km, 4 km, 6 km, and 8 km without intermixing.

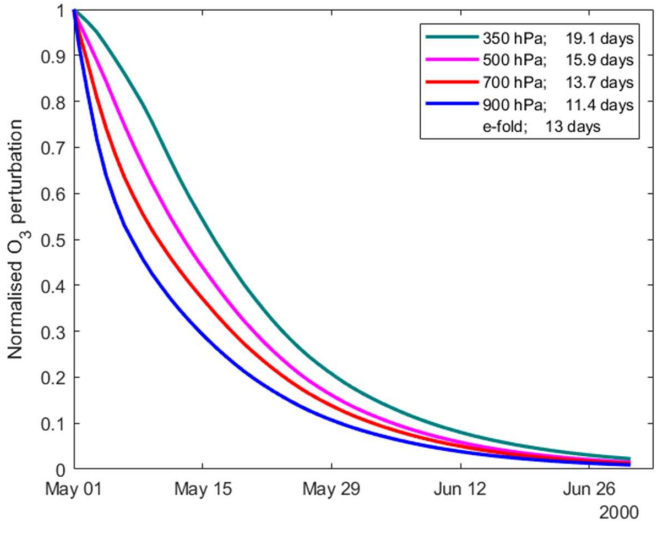

Figure 2: The decay of four CTM ozone releases at 1000-800 hPa (blue), 800-600 hPa (red), 600-400 hPa (magenta), and 400-300 hPa (green). Perturbations are normalised to the initial O_3 release. Ozone perturbations are diagnosed daily as diurnally averaged (between 00:00 UTC) grid-box masses and spatially integrated to obtain the perturbation lifetimes (legend). The area under each curve is the perturbation lifetime. The long-term unified decay-lifetime is around 13 days.

https://doi.org/10.5194/egusphere-2026-4590
Preprint. Discussion started: 21 August 2026

3 Results and discussion

The total pollution-driven changes in O_3 and CH_4 from the CTM and HMS can be directly compared, but the individual modelling stages of the HMS do not have a direct CTM analogue. The CTM can approximately emulate the BL-RL stage by integrating L-CH_4 and the O_3 perturbations (δO_3; Gmol day) in a box containing grid cells in the South Korean boundary layer (33°-39°N, 125-131°E, and layers 1-8, *i.e.*, >860 hPa). Boundary-layer (BL) pollution in the CTM disperses without a clear distinction between plumes (PL) and dispersed pollution (DP) as in the HMS. We define a PL box containing plumes in the CTM that extends the BL-RL box by 5° upwind to the West, 10° in the other directions, and from surface to 600 hPa. A distance of 10° represents about one day of transport at 10 m s^{-1}. The CTM BL box is embedded within this PL box and subtracted from the PL box budgets. The DP domain is the global atmosphere, subtracting the BL and PL budgets. These domains, and the CTM budget perturbations, are illustrated in Fig. 3.

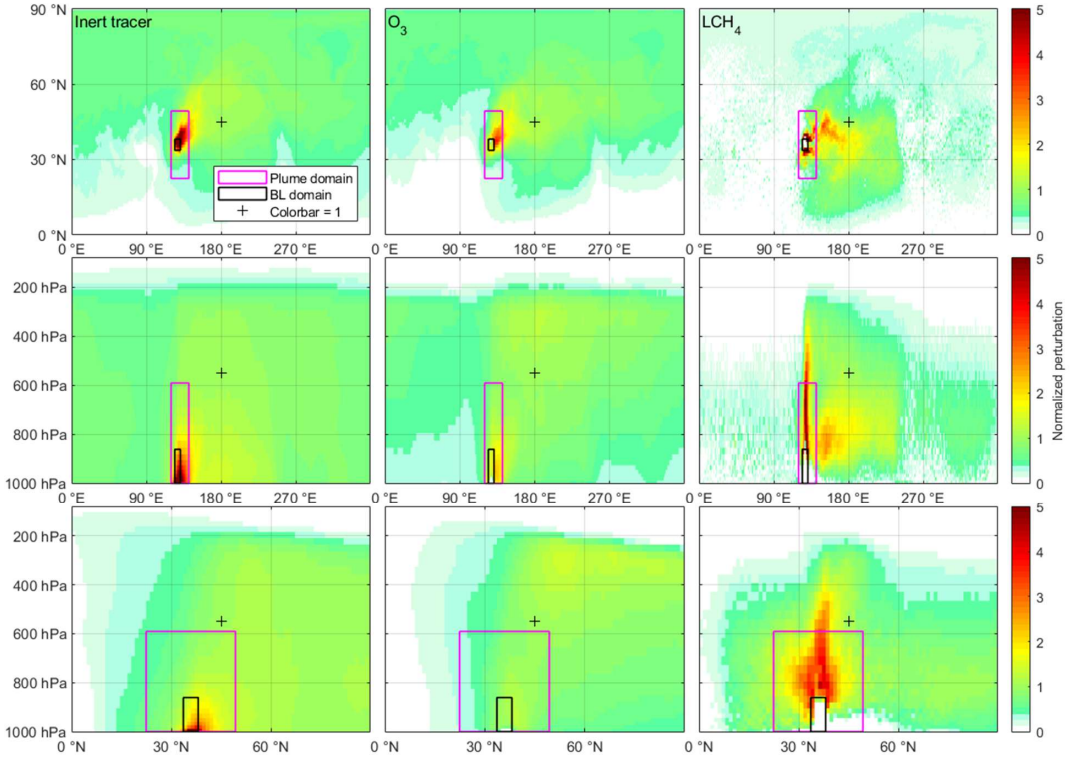

Figure 3: Time-integrated inert tracer abundance (left), integrated O_3 perturbation (middle), and CH_4 loss (L-CH4; right) over 92 days from the start of emissions. Inert tracer is emitted with a NO_x pattern over the 45-day emission period. Data are column densities (top) or mole fractions (centre and bottom) averaged over all latitudes (middle) or all longitudes (bottom). Prior to normalisation, inert tracer and O_3 data have units of mol m^{-2} day (top) and mol mol^{-1} day (middle and bottom), and L-CH_4 data have units of mol m^{-2} (top) and mol mol^{-1} (middle and bottom). All data are normalised to one at the map centre (+). Negative perturbations, *i.e.* in the Korean boundary-layer (black box) and plume region (purple box), are not shown.

https://doi.org/10.5194/egusphere-2026-4590
Preprint. Discussion started: 21 August 2026

3.1 Budgets

Table 2 shows the CTM and HMS budget terms (δO_3, P-O_3 and L-CH_4). The δO_3 mass perturbations are similar in both models and constitute a near steady-state +0.03 DU global O_3 enhancement during the 45-day emission period. The CTM P-O_3 is, however, only 71% that of the HMS (+22.2 *vs*. +31.2 Gmol) because the lifetime of an O_3 perturbation in the CTM is longer. The CTM CH_4 loss (L-CH_4) is also smaller at 47% that of HMS (+2.0 *vs*. +4.3 Gmol). The HMS calculation is based on 3-day aging for the PL stage before dispersion; if we assume 1-day plumes, the model discrepancies widen by about 10 percentage points (see Table 2). With 1-day plumes, the partitioning of L-CH_4 between PL and DP stages is similar in both models and likely reflects the size of PL diagnostic box in the CTM, which is based on one-day of transport distance. The dilution of emissions into coarser CTM grid-cells should nominally raise P-O_3 and L-CH_4 over the fine-grid HMS (*e.g.*, Charlton-Perez *et al*., 2009; Holmes *et al.*, 2014), but our results show the opposite. We attribute this to the very different VOC mechanisms. To compare the atmospheric compositions in the models, we examine the CTM control run (without the 10% added KORUS emissions) and the HMS pollution run, both of which simulate full South Korean emissions. The OH mole fraction in the entire BL domain, sampled over the first 10 days, is 0.06 ppt in the CTM *vs*. 0.11 ppt in the HMS. This is, once again, unexpected because mixing pollution over the coarse-grid CTM should raise OH (Li *et al.*, 2023). The HO_2 mole fraction (the dominant component of HO_x = HO_2 + OH) is similar in both models (4.2 *vs.* 4.4 ppt, respectively) with about the same overall loss frequency (1/49 *vs.* 1/56 s^{-1}) for radical-radical termination (*i.e.*, excluding OH-VOC reactions). However, the dominant termination reaction in the CTM is H_2O_2 formation, whereas in the HMS, it is HNO_3 formation.

As the pollution plumes age after leaving the BL, NO_x decays faster than VOCs, and ozone production efficiency rises (OPE = moles of O_3 produced per moles of HNO_3 formed; Liu *et al.*, 1987). In the HMS, the greatest, but not the most efficient, daily O_3 production is driven by the intense NO_x-VOC chemistry on day 1 of the PL stage (+8.0 Gmol at 7.6 OPE). Days 2 and 3 produce a combined +8.3 Gmol O_3 at 19.9 and 20.9 respective OPEs. At this stage, most of the reactive NO_x comes from organic nitrate decomposition. After day 3, in the DP stage, the dispersed plumes produce +10.9 Gmol O_3, at 27.8 OPE (NO_x alone) or 35.3 OPE (all pollution). The OPE over the full emission lifespan is 8.9. Over the combined PL and DP domains of the CTM, the OPE is 17.1, and over the full pollution lifespan, it is 6.3. The lower total OPE of the CTM is explained by the NO_x budget. Both models emit a total of 3.51 Gmol NO_x to the BL over 45 days. Of these emissions, the HMS exports 1.27 Gmol NO_x plus 0.47 Gmol organic nitrates (including 0.25 Gmol PAN) to the PL stage as plumes. The PL NO_x then decays to 0.08 Gmol by end of day 1 while organic nitrates increase to 0.60 Gmol (0.39 Gmol PAN). The CTM, on the other hand, exports 1.17 Gmol NO_x and just 0.08 Gmol PAN to the PL domain. The CTM pollution exiting the PL domain contains 0.22 Gmol NO_x and 0.12 Gmol PAN. The low yield of PAN in the CTM greatly reduces the amount of NO_x that reaches the clean, higher OPE environment. A study of US NO_x pollution during July computed a total OPE of 7 in the global troposphere (Jacob *et al*., 1993) which intermediates our CTM and HMS values. High PAN abundance in the boundary-layer was a noted problem in the US study, in contrast with the low PAN over South Korea (see Figure 1).

https://doi.org/10.5194/egusphere-2026-4590
Preprint. Discussion started: 21 August 2026

We analyse L-CH_4 by defining methane destruction efficiency similarly to OPE (MDE = moles of CH_4 lost per moles of HNO_3 formed; Holmes *et al.*, 2014). In the HMS, the total MDE is 1.2 over the whole model. The MDEs in the individual model stages are: 0.2 in the BL; 0.5, 2.4, and 3.5 on days 1-3 of PL aging; and 10.0 (NO_x alone) in the DP stage, or 7.3 (all pollution). In the CTM, the overall MDE is 0.6, with negative MDE in the BL (-0.1), 0.2 MDE in the PL, and 9.1 MDE in the DP domain. The overall range of MDEs is similar to that of the HMS. We once again attribute the low L-CH_4 in the CTM *vs*. HMS to low organic nitrate yield.

Compared with a maritime shipping plume study (Holmes *et al.*, 2014), the HMS OPEs and MDEs are similar. In fresh shipping plumes (<0.5 day-aged), the respective OPEs and MDEs are 1.7 and 0.4; and globally, they are 8.5 and 3.1. Overall, our MDEs are lower because the CO:NO_x ratio of South Korean emissions is 10 times greater than that of the shipping emissions in Holmes *et al*. (2014). The efficiency terms are defined with respect to NO_x loss; however, the O_3 and OH chemistry is sensitive to the co-emitted VOC and CO pollution.

Table 2: Methane and ozone budgets from the KORUS-AQ period of emissions.

Time-integrated diagnostics	**CTM**				**HMS: 3 days (1 day) plume aging**			
	Total	**BL box**	**PL box**	**DP region**	**Total**	**BL-RL**	**PL**	**DP**
L-CH_4 (Gmol)	+2.0	-0.2	+0.2	+2.0	+4.3 (+5.8)	+0.3	+1.7 (+0.5)	+2.3 (+5.0)
P-O_x (Gmol)	+21.4	+3.0	+6.6	+11.8	N/A	N/A	N/A	N/A
L-O_x (Gmol)	+15.1	+0.0	+1.5	+13.6	N/A	N/A	N/A	N/A
δO_3 (Gmol days)	+327	+1	+14	+312	+320 (+389)	+2	+34 (+8)	+284 (+379)
P-O_3 (Gmol)	+22.2	+0.1	+22.1		+31.2 (+35.8)	+4.0	+16.3 (+8.0)	+10.9 (+23.8)
OPE	6.3	0.0	17.7		8.9 (10.2)	2.3	11.2 (7.6)	27.8
MDE	0.6	-0.1	0.2	9.1	1.2 (1.7)	0.2	1.2 (0.4)	10.0

UCI-CTM diagnostics were calculated for a 10% KORUS-AQ emission perturbation (KORUS v5 + GFED5) in a 6°x6° degree box (100 km resolution), scaled to 100% by a factor of 10. The hybrid modelling system diagnostics were calculated for a 100% perturbation of the same emissions, but at 10 km resolution. The UCI-CTM model was run for 45 emission days + 47 spin-down days, after which the residuals were extrapolated via a least-squares exponential fit. In the CTM, the 'BL' (33°-39°N, 125-131°E, ＞860 hPa), 'PL' (23°-49°N, 120-141°E, 860-600 hPa), and 'dispersed' (global excluding 'BL' and 'plume' boxes) domains are spatial regions. In the hybrid model, these domains

https://doi.org/10.5194/egusphere-2026-4590
Preprint. Discussion started: 21 August 2026

are separate modelling stages featuring chemistry, emissions, and transport in the terrestrial South Korean boundary layer and residual layer (BL), chemical integration on plumes transported offshore (PL), and dilute linearised chemistry of three-day-aged plumes (DP).

3.2 Radiative Forcing

We compute the steady-state effective radiative forcing (ERF) from the integrated O_3 and CH_4 perturbations sustained during the 45-day emission period studied here. The chemical perturbations occur out to 120 days with the remaining O_3 perturbations decaying within a month but with the accumulated CH_4 perturbations decaying over the perturbation lifetime for global CH_4 of 12.4 years (Prather *et al.*, 2012). The global steady-state δO_3 enhancement per day of emissions is 0.03 DU in both models, calculated from time-integrated perturbation from initial emissions to final decay in DU-days divided by 45 days. At the end of the chemical integration the accumulated δCH_4 perturbations are 11.6 ppt in the CTM and 25.0 ppt in the HMS. To derive the steady-state δCH_4 sustained by the emissions, we divide the accumulated δCH_4 by 45 days and then multiply by 12.4 years to obtain -1.17 ppb and -2.52 ppb respectively.

The O_3 ERF is a combination of the spatially resolved δO_3 in the CTM with the May-to-August averaged ERF kernels from Oslo CTM (Søvde et al., 2012), mapping the Oslo 5.5° resolution onto the 1.1° UCI CTM grid via nearest neighbour interpolation. The per-day O_3 ERF is +1.13 mW m^{-2}. The CH_4 ERF uses the errata-corrected value from IPCC AR6 WGI (550 mW m^{-2} ppm^{-1}), which includes induced stratospheric H_2O and tropospheric O_3 increases, plus tropospheric feedbacks. Thus, the per-day CH_4 ERFs are -0.64 and -1.38 mW m^{-2}, for CTM and HMS respectively. The combined per-day ERFs are therefore +0.49 and -0.25 mW m^{-2}, respectively.

4 Conclusion

We benchmark the production of O_3 and destruction of CH_4 caused by 45 days of South Korean air pollution using the UCI global chemistry-transport model (CTM) against a hybrid modelling system (HMS). The CTM adopts a simplified chemical mechanism designed for clean-air chemistry. The HMS has extremely detailed chemical mechanisms but simplifies the transport and mixing of pollution after it departs the boundary-layer. The models produce similar integrated δO_3 mass perturbations, both equivalent to a steady-state +0.03 DU global enhancement over the 45-day emission period. However, the net O_3 production in the CTM is 71% that of the HMS because of the different O_3 lifetimes in each model. The CTM loss of CH_4 is half that of HMS. Combining O_3 increases (warming) with CH_4 decreases (cooling), the emissions cause net warming in the CTM (+0.49 mW m^{-2} per-day ERF) and net cooling in the HMS (-0.25 mW m^{-2}).

The smaller overall CTM perturbations to both O_3 and CH_4 reactivities are surprising because, nominally, we expect coarser resolution to rapidly dilute NO_x pollution and enhance the GHG reactivities (*e.g.*, Charlton-Perez *et al.*, 2009; Holmes *et al.*, 2014). Instead, we find that (1) the Korean NO_x pollution is intense enough to suppress O_3 in some 100-km grid cells, lowering local OPE and enhancing HNO_3 production in the boundary layer and (2) the low VOC reactivity in the CTM causes low PAN yields in the polluted air, hence less NO_x reaches the cleaner atmosphere where OPE and MDE are high. The role of PAN in

https://doi.org/10.5194/egusphere-2026-4590
Preprint. Discussion started: 21 August 2026

transporting pollution NO_x to the free troposphere and thus altering the oxidising capacity of the atmosphere is well recognized (e.g., Singh, 1987; Hudman et al., 2004), and this work emphasizes the consequences for the O_3 and CH_4 budgets.

South Korean air pollution is notably rich in aromatic species, which increase PAN (and other organic nitrates) when included in the chemical mechanism (Fischer *et al.*, 2014; Oak *et al.*, 2019), and this is found with our HMS chemistry. Adopting the MCM mechanism in the CTM is not feasible, but introducing aromatic surrogates for toluene and the xylene family would improve OH-VOC chemistry and increase PAN production. The HMS performs a reasonably seamless chemical integration over the boundary-layer and offshore plumes; however, the instantaneous dispersion in the free troposphere creates a sharp discontinuity in the chemical environment which enhances P-O_3 and L-CH_4 to an unknown degree. The transition could instead be mediated by background-air dilution steps, interspersed with chemistry steps, using theoretical dilution timescales (*e.g.*, Prather and Jaffe, 1990). Evaluating the dynamical lifespans of pollution plumes, *i.e.*, until the onset of rapid background mixing, is a challenging problem and was found to be a major source of uncertainty in HMS budgets (Wilson and Prather, 2026). Another HMS issue is the fixed clean-air boundary condition imposed on free tropospheric air entering the BL; this approach fails to account for transboundary pollution. A time-varying background composition could be derived from assimilated chemical data (*e.g.*, Miyazaki *et al.*, 2019), although such data is limited for species that are not remotely sensed.

Our results suggest that skilful modelling of organic nitrate chemistry is a requirement for obtaining correct CH_4 and O_3 budgets. Field campaigns such as KORUS-AQ and the recent Airborne and Satellite Investigation of Asian Air Quality (ASIA-AQ) mission (Crawford *et al.*, 2022) provide useful model diagnostics (*e.g.* speciated organic nitrates) for atmospheric chemistry simulations in intensely polluted regions. A multi-model ensemble of pollution reactivities supported by airborne campaign data would give further insight into factors controlling the CH_4 and O_3 budgets and the generality of our conclusions here.

Code and data availability

All KORUS-AQ data used in this paper are available via https://doi.org/10.5067/Suborbital/KORUSAQ/DATA01 (KORUSAQ Science Team, 2019). Datasets for the CTM and HMS are available at Wilson (2026a) and Wilson (2026b) respectively.

Author contributions

CW ran the models, analysed the output, and wrote the paper. MP supervised the work, advised on the modelling, and edited the paper.

https://doi.org/10.5194/egusphere-2026-4590
Preprint. Discussion started: 21 August 2026

Competing interests

The contact author has declared that neither of the authors has any competing interests.

Acknowledgements

We acknowledge the Research Cyberinfrastructure Center of the University of California, Irvine, for managing the high-performance computing resources used in this work.

Financial support

This research has been supported by the National Aeronautics and Space Administration (grant no. 80NSSC21K1454) and the National Science Foundation (grant no. AGS-2135749).

References

Bloss, C., Wagner, V., Jenkin, M. E., Volkamer, R., Bloss, W. J., Lee, J. D., Heard, D. E., Wirtz, K., Martin-Reviejo, M., Rea, G., Wenger, J. C., and Pilling, M. J.: Development of a detailed chemical mechanism (MCMv3.1) for the atmospheric oxidation of aromatic hydrocarbons, Atmospheric Chemistry and Physics, 5, 641–664, https://doi.org/10.5194/acp-5-641-2005, 2005.

Carter, W. P. L.: Development of the SAPRC-07 chemical mechanism, Atmospheric Environment, 44, 5324–5335, https://doi.org/10.1016/j.atmosenv.2010.01.026, 2010.

Charlton-Perez, C. L., Evans, M. J., Marsham, J. H., and Esler, J. G.: The impact of resolution on ship plume simulations with NO_x chemistry, Atmospheric Chemistry and Physics, 9, 7505–7518, https://doi.org/10.5194/acp-9-7505-2009, 2009.

Chen, Y., Hall, J., van Wees, D., Andela, N., Hantson, S., Giglio, L., van der Werf, G. R., Morton, D. C., and Randerson, J. T.: Multi-decadal trends and variability in burned area from the fifth version of the Global Fire Emissions Database (GFED5), Earth System Science Data, 15, 5227–5259, https://doi.org/10.5194/essd-15-5227-2023, 2023.

Crawford, J. H., Ahn, J.-Y., Al-Saadi, J., Chang, L., Emmons, L. K., Kim, J., Lee, G., Park, J.-H., Park, R. J., Woo, J. H., Song, C.-K., Hong, J.-H., Hong, Y.-D., Lefer, B. L., Lee, M., Lee, T., Kim, S., Min, K.-E., Yum, S. S., Shin, H. J., Kim, Y.-W., Choi, J.-S., Park, J.-S., Szykman, J. J., Long, R. W., Jordan, C. E., Simpson, I. J., Fried, A., Dibb, J. E., Cho, S., and Kim, Y. P.: The Korea–United States Air Quality (KORUS-AQ) field study, Elementa: Science of the Anthropocene, 9, 00163, https://doi.org/10.1525/elementa.2020.00163, 2021.

Fischer, E. V., Jaffe, D. A., Reidmiller, D. R., and Jaeglé, L.: Meteorological controls on observed peroxyacetyl nitrate at Mount Bachelor during the spring of 2008, Journal of Geophysical Research: Atmospheres, 115, https://doi.org/10.1029/2009JD012776, 2010.

https://doi.org/10.5194/egusphere-2026-4590
Preprint. Discussion started: 21 August 2026

Fischer, E. V., Jacob, D. J., Yantosca, R. M., Sulprizio, M. P., Millet, D. B., Mao, J., Paulot, F., Singh, H. B., Roiger, A., Ries, L., Talbot, R. W., Dzepina, K., and Pandey Deolal, S.: Atmospheric peroxyacetyl nitrate (PAN): a global budget and source attribution, Atmos Chem Phys, 14, 2679–2698, https://doi.org/10.5194/acp-14-2679-2014, 2014.

Gaubert, B., Emmons, L. K., Raeder, K., Tilmes, S., Miyazaki, K., Arellano Jr., A. F., Elguindi, N., Granier, C., Tang, W., Barré, J., Worden, H. M., Buchholz, R. R., Edwards, D. P., Franke, P., Anderson, J. L., Saunois, M., Schroeder, J., Woo, J.-H., Simpson, I. J., Blake, D. R., Meinardi, S., Wennberg, P. O., Crounse, J., Teng, A., Kim, M., Dickerson, R. R., He, H., Ren, X., Pusede, S. E., and Diskin, G. S.: Correcting model biases of CO in East Asia: impact on oxidant distributions during KORUS-AQ, Atmospheric Chemistry and Physics, 20, 14617–14647, https://doi.org/10.5194/acp-20-14617-2020, 2020.

Guenther, A. B., Jiang, X., Heald, C. L., Sakulyanontvittaya, T., Duhl, T., Emmons, L. K., and Wang, X.: The Model of Emissions of Gases and Aerosols from Nature version 2.1 (MEGAN2.1): an extended and updated framework for modeling biogenic emissions, Geoscientific Model Development, 5, 1471–1492, https://doi.org/10.5194/gmd-5-1471-2012, 2012.

Guo, H., Flynn, C. M., Prather, M. J., Strode, S. A., Steenrod, S. D., Emmons, L., Lacey, F., Lamarque, J.-F., Fiore, A. M., Correa, G., Murray, L. T., Wolfe, G. M., St. Clair, J. M., Kim, M., Crounse, J., Diskin, G., DiGangi, J., Daube, B. C., Commane, R., McKain, K., Peischl, J., Ryerson, T. B., Thompson, C., Hanisco, T. F., Blake, D., Blake, N. J., Apel, E. C., Hornbrook, R. S., Elkins, J. W., Hintsa, E. J., Moore, F. L., and Wofsy, S. C.: Heterogeneity and chemical reactivity of the remote troposphere defined by aircraft measurements – corrected, Atmospheric Chemistry and Physics, 23, 99–117, https://doi.org/10.5194/acp-23-99-2023, 2023.

Gaudel, A., Cooper, O. R., Ancellet, G., Barret, B., Boynard, A., Burrows, J. P., Clerbaux, C., Coheur, P.-F., Cuesta, J., Cuevas, E., Doniki, S., Dufour, G., Ebojie, F., Foret, G., Garcia, O., Granados-Muñoz, M. J., Hannigan, J. W., Hase, F., Hassler, B., Huang, G., Hurtmans, D., Jaffe, D., Jones, N., Kalabokas, P., Kerridge, B., Kulawik, S., Latter, B., Leblanc, T., Le Flochmoën, E., Lin, W., Liu, J., Liu, X., Mahieu, E., McClure-Begley, A., Neu, J. L., Osman, M., Palm, M., Petetin, H., Petropavlovskikh, I., Querel, R., Rahpoe, N., Rozanov, A., Schultz, M. G., Schwab, J., Siddans, R., Smale, D., Steinbacher, M., Tanimoto, H., Tarasick, D. W., Thouret, V., Thompson, A. M., Trickl, T., Weatherhead, E., Wespes, C., Worden, H. M., Vigouroux, C., Xu, X., Zeng, G., and Ziemke, J.: Tropospheric Ozone Assessment Report: Present-day distribution and trends of tropospheric ozone relevant to climate and global atmospheric chemistry model evaluation, Elementa: Science of the Anthropocene, 6, 39, https://doi.org/10.1525/elementa.291, 2018.

Hoesly, R. M., Smith, S. J., Feng, L., Klimont, Z., Janssens-Maenhout, G., Pitkanen, T., Seibert, J. J., Vu, L., Andres, R. J., Bolt, R. M., Bond, T. C., Dawidowski, L., Kholod, N., Kurokawa, J., Li, M., Liu, L., Lu, Z., Moura, M. C. P., O'Rourke, P. R., and Zhang, Q.: Historical (1750–2014) anthropogenic emissions of reactive gases and aerosols from the Community Emissions Data System (CEDS), Geoscientific Model Development, 11, 369–408, https://doi.org/10.5194/gmd-11-369-2018, 2018.

Holmes, C. D., Prather, M. J., and Vinken, G. C. M.: The climate impact of ship NO_x emissions: an improved estimate accounting for plume chemistry, Atmospheric Chemistry and Physics, 14, 6801–6812, https://doi.org/10.5194/acp-14-6801-2014, 2014.

https://doi.org/10.5194/egusphere-2026-4590
Preprint. Discussion started: 21 August 2026

Hudman, R. C., Jacob, D. J., Cooper, O. R., Evans, M. J., Heald, C. L., Park, R. J., Fehsenfeld, F., Flocke, F., Holloway, J., Hübler, G., Kita, K., Koike, M., Kondo, Y., Neuman, A., Nowak, J., Oltmans, S., Parrish, D., Roberts, J. M., and Ryerson, T.: Ozone production in transpacific Asian pollution plumes and implications for ozone air quality in California, Journal of Geophysical Research: Atmospheres, 109, https://doi.org/10.1029/2004JD004974, 2004.

Isaksen, I. S. A. and Hov, Ø.: Calculation of trends in the tropospheric concentration of O3, OH, CO, CH4 and NOx | Tellus B: Chemical and Physical Meteorology, https://doi.org/10.3402/tellusb.v39i3.15347, 2022.

Jacob, D. J., Logan, J. A., Gardner, G. M., Yevich, R. M., Spivakovsky, C. M., Wofsy, S. C., Sillman, S., and Prather, M. J.: Factors regulating ozone over the United States and its export to the global atmosphere, https://doi.org/10.1029/98JD01224, 1993.

Jenkin, M. E., Saunders, S. M., and Pilling, M. J.: The tropospheric degradation of volatile organic compounds: a protocol for mechanism development, Atmospheric Environment, 31, 81–104, https://doi.org/10.1016/S1352-2310(96)00105-7, 1997.

Jenkin, M. E., Saunders, S. M., Wagner, V., and Pilling, M. J.: Protocol for the development of the Master Chemical Mechanism, MCM v3 (Part B): tropospheric degradation of aromatic volatile organic compounds, Atmospheric Chemistry and Physics, 3, 181–193, https://doi.org/10.5194/acp-3-181-2003, 2003.

Jenkin, M. E., Young, J. C., and Rickard, A. R.: The MCM v3.3.1 degradation scheme for isoprene, Atmospheric Chemistry and Physics, 15, 11433–11459, https://doi.org/10.5194/acp-15-11433-2015, 2015.

Kim, K.-M., Kim, S.-W., Seo, S., Blake, D. R., Cho, S., Crawford, J. H., Emmons, L. K., Fried, A., Herman, J. R., Hong, J., Jung, J., Pfister, G. G., Weinheimer, A. J., Woo, J.-H., and Zhang, Q.: Sensitivity of the WRF-Chem v4.4 simulations of ozone and formaldehyde and their precursors to multiple bottom-up emission inventories over East Asia during the KORUS-AQ 2016 field campaign, Geoscientific Model Development, 17, 1931–1955, https://doi.org/10.5194/gmd-17-1931-2024, 2024.

KORUS-AQ Science Team: KORUS-AQ NASA DC-8 airborne 10 s merged data revision 6 – ICARTT Files, NASA Langley Atmospheric Science Data Center DAAC [data set], https://doi.org/10.5067/Suborbital/KORUSAQ/DATA01, 2019.

Li, C., Martin, R. V., Cohen, R. C., Bindle, L., Zhang, D., Chatterjee, D., Weng, H., and Lin, J.: Variable effects of spatial resolution on modeling of nitrogen oxides, Atmospheric Chemistry and Physics, 23, 3031–3049, https://doi.org/10.5194/acp-23-3031-2023, 2023.

Liu, S. C., Trainer, M., Fehsenfeld, F. C., Parrish, D. D., Williams, E. J., Fahey, D. W., Hübler, G., and Murphy, P. C.: Ozone production in the rural troposphere and the implications for regional and global ozone distributions, Journal of Geophysical Research: Atmospheres, 92, 4191–4207, https://doi.org/10.1029/JD092iD04p04191, 1987.

Miyazaki, K., Sekiya, T., Fu, D., Bowman, K. W., Kulawik, S. S., Sudo, K., Walker, T., Kanaya, Y., Takigawa, M., Ogochi, K., Eskes, H., Boersma, K. F., Thompson, A. M., Gaubert, B., Barre, J., and Emmons, L. K.: Balance of Emission and Dynamical Controls on Ozone During the Korea-United States Air Quality Campaign From Multiconstituent Satellite Data Assimilation, Journal of Geophysical Research: Atmospheres, 124, 387–413, https://doi.org/10.1029/2018JD028912, 2019.

Myhre, G., D. Shindell, F.-M. Bréon, W. Collins, J. Fuglestvedt, J. Huang, D. Koch, J.-F. Lamarque, D. Lee, B. Mendoza, T. Nakajima, A. Robock, G. Stephens, T. Takemura and H. Zhang, 2013: Anthropogenic and Natural Radiative Forcing. In:

https://doi.org/10.5194/egusphere-2026-4590
Preprint. Discussion started: 21 August 2026

Climate Change 2013: The Physical Science Basis. Contribution of Working Group I to the Fifth Assessment Report of the Intergovernmental Panel on Climate Change [Stocker, T.F., D. Qin, G.-K. Plattner, M. Tignor, S.K. Allen, J. Boschung, A. Nauels, Y. Xia, V. Bex and P.M. Midgley (eds.)]. Cambridge University Press, Cambridge, United Kingdom and New York, NY, USA.

Oak, Y. J., Park, R. J., Schroeder, J. R., Crawford, J. H., Blake, D. R., Weinheimer, A. J., Woo, J.-H., Kim, S.-W., Yeo, H., Fried, A., Wisthaler, A., and Brune, W. H.: Evaluation of simulated O3 production efficiency during the KORUS-AQ campaign: Implications for anthropogenic NOx emissions in Korea, Elementa: Science of the Anthropocene, 7, 56, https://doi.org/10.1525/elementa.394, 2019.

Prather, M. J.: The Spillover of Tropospheric Ozone Increases Has Hidden the Extent of Stratospheric Ozone Depletion by Halogens, AGU Advances, 5, e2023AV001154, https://doi.org/10.1029/2023AV001154, 2024.

Prather, M. J.: Calibrating the Tropospheric Air and Ozone Mass, AGU Advances, 6, e2025AV001651, https://doi.org/10.1029/2025AV001651, 2025.

Prather, M. and Jaffe, A. H.: Global impact of the Antarctic ozone hole: Chemical propagation, Journal of Geophysical Research: Atmospheres, 95, 3473–3492, https://doi.org/10.1029/JD095iD04p03473, 1990.

Prather, M. J. and Zhu, X.: Lifetimes and timescales of tropospheric ozone, Elementa: Science of the Anthropocene, 12, 00112, https://doi.org/10.1525/elementa.2023.00112, 2024.

Prather, M. J., Holmes, C. D., and Hsu, J.: Reactive greenhouse gas scenarios: Systematic exploration of uncertainties and the role of atmospheric chemistry, Geophysical Research Letters, 39, https://doi.org/10.1029/2012GL051440, 2012.

Saunders, S. M., Jenkin, M. E., Derwent, R. G., and Pilling, M. J.: Protocol for the development of the Master Chemical Mechanism, MCM v3 (Part A): tropospheric degradation of non-aromatic volatile organic compounds, Atmospheric Chemistry and Physics, 3, 161–180, https://doi.org/10.5194/acp-3-161-2003, 2003.

Saunois, M., Martinez, A., Poulter, B., Zhang, Z., Raymond, P. A., Regnier, P., Canadell, J. G., Jackson, R. B., Patra, P. K., Bousquet, P., Ciais, P., Dlugokencky, E. J., Lan, X., Allen, G. H., Bastviken, D., Beerling, D. J., Belikov, D. A., Blake, D. R., Castaldi, S., Crippa, M., Deemer, B. R., Dennison, F., Etiope, G., Gedney, N., Höglund-Isaksson, L., Holgerson, M. A., Hopcroft, P. O., Hugelius, G., Ito, A., Jain, A. K., Janardanan, R., Johnson, M. S., Kleinen, T., Krummel, P. B., Lauerwald, R., Li, T., Liu, X., McDonald, K. C., Melton, J. R., Mühle, J., Müller, J., Murguia-Flores, F., Niwa, Y., Noce, S., Pan, S., Parker, R. J., Peng, C., Ramonet, M., Riley, W. J., Rocher-Ros, G., Rosentreter, J. A., Sasakawa, M., Segers, A., Smith, S. J., Stanley, E. H., Thanwerdas, J., Tian, H., Tsuruta, A., Tubiello, F. N., Weber, T. S., van der Werf, G. R., Worthy, D. E. J., Xi, Y., Yoshida, Y., Zhang, W., Zheng, B., Zhu, Q., Zhu, Q., and Zhuang, Q.: Global Methane Budget 2000–2020, Earth System Science Data, 17, 1873–1958, https://doi.org/10.5194/essd-17-1873-2025, 2025.

Sindelarova, K., Granier, C., Bouarar, I., Guenther, A., Tilmes, S., Stavrakou, T., Müller, J.-F., Kuhn, U., Stefani, P., and Knorr, W.: Global data set of biogenic VOC emissions calculated by the MEGAN model over the last 30 years, Atmospheric Chemistry and Physics, 14, 9317–9341, https://doi.org/10.5194/acp-14-9317-2014, 2014.

https://doi.org/10.5194/egusphere-2026-4590
Preprint. Discussion started: 21 August 2026

Singh, H. B.: Reactive nitrogen in the troposphere, Environ. Sci. Technol., 21, 320–327, https://doi.org/10.1021/es00158a001, 1987.

Stevenson, D. S., Zhao, A., Naik, V., O'Connor, F. M., Tilmes, S., Zeng, G., Murray, L. T., Collins, W. J., Griffiths, P. T., Shim, S., Horowitz, L. W., Sentman, L. T., and Emmons, L.: Trends in global tropospheric hydroxyl radical and methane lifetime since 1850 from AerChemMIP, Atmospheric Chemistry and Physics, 20, 12905–12920, https://doi.org/10.5194/acp-20-12905-2020, 2020.

Szopa, S., V. Naik, B. Adhikary, P. Artaxo, T. Berntsen, W.D. Collins, S. Fuzzi, L. Gallardo, A. Kiendler-Scharr, Z. Klimont, H. Liao, N. Unger, and P. Zanis, 2021: Short-Lived Climate Forcers. In Climate Change 2021: The Physical Science Basis. Contribution of Working Group I to the Sixth Assessment Report of the Intergovernmental Panel on Climate Change [Masson-Delmotte, V., P. Zhai, A. Pirani, S.L. Connors, C. Péan, S. Berger, N. Caud, Y. Chen, L. Goldfarb, M.I. Gomis, M. Huang, K. Leitzell, E. Lonnoy, J.B.R. Matthews, T.K. Maycock, T. Waterfield, O. Yelekçi, R. Yu, and B. Zhou (eds.)]. Cambridge University Press, Cambridge, United Kingdom and New York, NY, USA, pp. 817–922, doi: 10.1017/9781009157896.008.

Wild, O., Prather, M. J., Akimoto, H., Sundet, J. K., Isaksen, I. S. A., Crawford, J. H., Davis, D. D., Avery, M. A., Kondo, Y., Sachse, G. W., and Sandholm, S. T.: Chemical transport model ozone simulations for spring 2001 over the western Pacific: Regional ozone production and its global impacts, Journal of Geophysical Research: Atmospheres, 109, https://doi.org/10.1029/2003JD004041, 2004.

Wilson, C.: Methane loss (L-CH_4) and tropospheric ozone (O_3) burden in response to a 10% KORUS-AQ emission perturbation in the UCI chemistry-transport model, Dryad [dataset], https://doi.org/10.5061/dryad.djh9w0wgm, 2026a.

Wilson, C.: Modelling system for computing the tropospheric O3 and CH4 perturbations from South Korean Emissions (KORUS-AQ period), Dryad [code], https://doi.org/10.5061/dryad.f4qrfj78x, 2026b.

Wilson, C. P. and Prather, M. J.: Life–cycle impacts of South Korean air pollution on tropospheric ozone and methane: sensitivity to dispersion time, Atmospheric Chemistry and Physics, 26, 3995–4017, https://doi.org/10.5194/acp-26-3995-2026, 2026.

Woo, J.-H., Kim, Y., Kim, H.-K., Choi, K.-C., Eum, J.-H., Lee, J.-B., Lim, J.-H., Kim, J., and Seong, M.: Development of the CREATE Inventory in Support of Integrated Climate and Air Quality Modeling for Asia, Sustainability, 12, 7930, https://doi.org/10.3390/su12197930, 2020.

Zakoura, M. and Pandis, S. N.: Overprediction of aerosol nitrate by chemical transport models: The role of grid resolution, Atmospheric Environment, 187, 390–400, https://doi.org/10.1016/j.atmosenv.2018.05.066, 2018.

Ziemke, J. R., Oman, L. D., Strode, S. A., Douglass, A. R., Olsen, M. A., McPeters, R. D., Bhartia, P. K., Froidevaux, L., Labow, G. J., Witte, J. C., Thompson, A. M., Haffner, D. P., Kramarova, N. A., Frith, S. M., Huang, L.-K., Jaross, G. R., Seftor, C. J., Deland, M. T., and Taylor, S. L.: Trends in global tropospheric ozone inferred from a composite record of TOMS/OMI/MLS/OMPS satellite measurements and the MERRA-2 GMI simulation, Atmospheric Chemistry and Physics, 19, 3257–3269, https://doi.org/10.5194/acp-19-3257-2019, 2019.